Applied Thermal Engineering 48 (2012) 81–88

Contents lists available at SciVerse ScienceDirect

Applied Thermal Engineering

journal homepage: www.elsevier.com/locate/apthermeng

Numerical simulation of the thermal hydraulic performance of a plate pin fin heat sink

Wuhan Yuan [a], Jiyun Zhao [b], C.P. Tso [c], Tianhua Wu [a], Wei Liu [a], Tingzhen Ming [a,*]

[a] School of Energy and Power Engineering, Huazhong University of Science and Technology, No. 1037 Luoyu Road, Wuhan 430074, China
[b] EXQUISITUS, Centre for E-City, School of Electrical and Electronic Engineering, Nanyang Technological University, 639798 Singapore, Singapore
[c] Division of Thermal and Fluids Engineering, School of Mechanical and Aerospace Engineering, Nanyang Technological University, Singapore

HIGHLIGHTS

- Pin height and air velocity significantly influence thermal performance of PPFHS.
- Less influence by in-line or staggered array.
- Less influence by neighbor pin flow-directional center distance.
- Design with >6.5 m/s air can cool to <358 K, for desktop PC CPU with 2.20 W/cm^2 flux.

ARTICLE INFO

Article history:
Received 24 November 2011
Accepted 12 April 2012
Available online 9 May 2012

Keywords:
Plate pin fin heat sink
Electronics cooling simulation
Pressure drop
Thermal resistance
Profit factor

ABSTRACT

The computational fluid dynamic software FLUENT is used in assessing the electronics cooling potential of a plate pin fin heat sink (PPFHS), including the conjugate effect. The simulation results are validated with reported experimental data. The simulation shows that pin height and air velocity have significant influences on the thermal hydraulic performances of PPFHS while the influences of in-line/staggered array and neighbor pin flow-directional center distance (NPFDCD) of the PPFHS are less notable. In applying the present design to the cooling of a desktop PC CPU at a heat flux of 2.20 W/cm^2, the temperature can be kept at less than 358 K with an air velocity over 6.5 m/s.

1. Introduction

With the rapid advances in micro electromechanical systems (MEMS), the size of electronic components shrinks and the thermal power increases dramatically, resulting in high working temperatures that can greatly reduce the reliability of the components and shorten their service lives. Hence thermal management of electronic chips has been advancing in tandem, in order to control the working temperature to within acceptable limits by devising more effective ways to remove the waste heat. Devices such as heat pipes [1,2] and jet impingement cooling [3,4], have been studied. And although air has been a common coolant, liquid and flow boiling have also been considered [5,6].

Tuckerman and Peace in 1981 proposed the micro-channel heat sink (MCHS) cooling concept. They fabricated rectangle micro-channel heat sinks in silicon wafers, and using water as coolant, the MCHS was proved suitable for cooling such devices as high-performance microprocessors, laser diode arrays, radars and high-energy-laser mirrors [7,8]. The success motivated others to design better heat sinks, as attested by the following survey.

Chiang et al. [9] presented a systematic experimental design based on the response surface methodology to identify the effects of design parameters of the PFHS on the thermal performance, and explored various design parameters, such as the height and diameter of pin fin and the width of pitch between fins in the experiment. Cao and Chen [10] studied optimal design on MCHS for high power laser mirror, and suggested ways to improve on some physical parameters. Chen et al. [11] compared the performances of triangular, rectangular and trapezoidal MCHSs, while Leon et al. [12] conducted a numerical investigation on the heat sink with aerodynamic shaped cooling fins. Mohammed et al. [13,14] carried out numerical simulations to compare the zigzag, curvy, and step MCHSs and concluded that the zigzag design has the best thermal performance. For the wavy MCHS the temperature was always

* Corresponding author. Tel.: +86 27 87542618x608, fax: +86 27 87540724.
E-mail address: tzming@mail.hust.edu.cn (T. Ming).

1359-4311/$ – see front matter © 2012 Elsevier Ltd. All rights reserved.
doi:10.1016/j.applthermaleng.2012.04.029

Nomenclature

Latin symbols

A	Areas [m^2]
C	Constant in turbulent model
H	Height [m]
J	Profit factor [-]
L	Distance from base in x-direction [m]
$\dot{m}$	Mass flow rate [kg s^{-1}]
N	Fin number [-]
p	Pressure [pa]
E	Pumping power [W]
Q	Heating power [W]
R	Resistance [K W^{-1}]
Re	Reynolds number [-]
T	Temperature [K]
x, y, z	Cartesian coordinates
X, Y, Z	Dimensionless dartesian coordinates
U, V, W	Dimensionless velocity
P	Dimensionless pressure

Greek symbols

σ	Constant in turbulent model
δ	Fin spacing [mm]
Δ	Differential
μ	Viscosity [m s^{-2}]
ρ	Density [kg m^{-3}]
θ	Dimensionless temperature

Subscripts

i, j	Repeated-subscript indices
in	Inlet
t	Turbulent flow
out	Outlet
th	Thermal
p	Flow passage
s	Solid
w	Wall
f	Fluid

lower than that of plate-fin heat sink (PFHS). Wang et al. [15] studied the effect of cannelure fin configuration on MCHS. Reyes et al. [16] experimentally studied MCHS with tip clearance and claimed it to be a favorable option for MCHS. Yin et al. [17] experimentally applied the composite PCM to a heat sink to improve resistance to high heat flux shocks and to ensure reliability and stability. Later, Sabbah et al. [18] adopted micro-encapsulated phase change material (MEPCM) to enhance the performance of MCHS. Shaeri and Yaghoubi [19] numerically studied perforated fins, which gave better performance and also had weight reduction. Xie et al. [20] presented a heat pipe heat sink with a novel wick structure. Liang and Hung [21] experimented with finned U-shaped heat pipes and concluded that the optimal L-ratio of U-shape heat pipes is dependent on factors like fin spacing and heat pipe diameter. Li et al. [22] studied the plate-fin heat sink under impingement cooling. Ho et al. [23] used Al_2O_3/water nano-fluid as coolant in MCHS cooling experiments, with significantly better heat transfer while the friction factor increased only slightly.

Although the PFHS is simple and low cost, the intrinsic shortcoming is that parallel plate fins make airflows smoother, which is undesirable for enhancing heat transfer performances [24]. To improve the heat transfer, the plate pin fin heat sink (PPFHS) was proposed, which is constructed by designing several pin fins in the flow passages of PFHS, and is thus a combination of pin fin arrays and PFHS. Experimental research of in-line and staggered pin fin arrays was reported in 1980 by Sparrow et al. [25], who showed that the heat transfer coefficient for the staggered array was higher than those for the in-line one, but the pressure drop was also higher. The in-line array transfers more heat for the same pumping power and heat transfer area, but the staggered array requires less surface heat load and mass flow rate. Yu et al. [24,26,27] studied PPFHS numerically and experimentally, and found that PPFHS had advantages over PFHS in heat transfer performance while the pressure drop of the former was much higher, and overall PPFHS was superior. Yang and Peng [28] examined the effect of the mixed-height pin-fin design on the PPFHS, and showed that the plate-circular pin-fin heat sink has better overall performance than the plate fin heat sink.

Hence, PPFHS generally out-performs PFHS although the manufacturing costs of both types are about the same. There is still a lot to be studied on the thermal and hydraulic performances of various configurations of the PPFHS. Qu and Mudawar [8] showed that the conventional Navier–Stokes and energy equations can adequately predict the fluid flow and heat transfer characteristics of micro-channel heat sinks, and therefore CFD studies are valuable. In this paper, we will compare our CFD results with the experimental results of Yu et al. [24,26,27] and Yang and Peng [28]. The aim is to find the key parameters that influence the thermal and hydraulic performances of PPFHS and to find the potential application to the desktop PC CPU.

2. Theory

2.1. Model development

The basic geometrical parameters of the models in this paper are based on Yu et al. [22,24], and shown in Fig. 1 and Table 1, respectively. Different types of PPFHS are analyzed through numerical simulation. The nearest distance between the pin center and fin wall is set as one-diameter (1D) and the neighbor-pins' flow-directional center distances (NPFDCD) of 4D, 6D, 8D, 10D and 12D are adopted. The four types of PPFHS with different pin–diameter combinations are also studied, with dimensions as shown in Table 2.

2.2. Computational domain and simulation settings

Given the periodic structure of the heat sinks, only one flow passage is investigated. The computational domain employed is shown in Fig. 2. The material of the heat sink is aluminum. The bottom of the computational domain is heated at a constant heat transfer rate of 10 W, that is, the heat flux at the fin base is 3665 W/m^2.The flow is assumed to be three-dimensional, incompressible, steady, turbulent, and since the heating is low, constant air properties. Radiation effect is ignored.

2.3. Mathematical model

As shown in the geometrical model, both fluid and solid region take part in the conjugate simulation of plate pin fin heat sink. The standard$k-\varepsilon$model is adopted to describe the turbulent fluid flow in the flow passage. The governing equations are set as follows [29]:

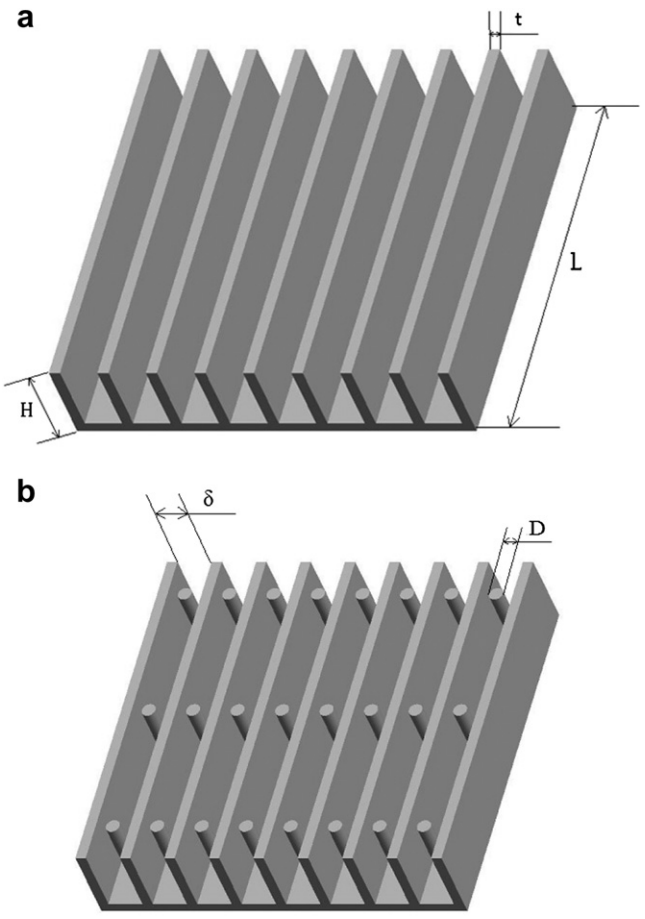

Fig. 1. Schematic diagrams of PFHS and PPFHS: (a) Plate fin heat sink (b) Plate-pin fin heat sink.

Continuity equation:

$$\frac{\partial U}{\partial X}+\frac{\partial V}{\partial Y}+\frac{\partial W}{\partial Z}=0 \tag{1}$$

Momentum equation:

$$\left(U\frac{\partial U}{\partial X}+V\frac{\partial U}{\partial Y}+W\frac{\partial U}{\partial Z}\right)=-\frac{dP}{dX}+\frac{1}{\mathrm{Re}}\left(\frac{\partial^2 U}{\partial X^2}+\frac{\partial^2 U}{\partial Y^2}+\frac{\partial^2 U}{\partial Z^2}\right) \tag{2}$$

$$\left(U\frac{\partial V}{\partial X}+V\frac{\partial V}{\partial Y}+W\frac{\partial V}{\partial Z}\right)=-\frac{dP}{dY}+\frac{1}{\mathrm{Re}}\left(\frac{\partial^2 V}{\partial X^2}+\frac{\partial^2 V}{\partial Y^2}+\frac{\partial^2 V}{\partial Z^2}\right) \tag{3}$$

$$\left(U\frac{\partial \theta}{\partial X}+V\frac{\partial \theta}{\partial Y}+W\frac{\partial \theta}{\partial Z}\right)=\frac{1}{\mathrm{Re}\cdot\mathrm{Pr}}\left(\frac{\partial^2 \theta}{\partial X^2}+\frac{\partial^2 \theta}{\partial Y^2}+\frac{\partial^2 \theta}{\partial Z^2}\right) \tag{4}$$

Energy equation:

$$\left(U\frac{\partial \theta}{\partial X}+V\frac{\partial \theta}{\partial Y}+W\frac{\partial \theta}{\partial Z}\right)=\frac{1}{\mathrm{Re}\cdot\mathrm{Pr}}\left(\frac{\partial^2 \theta}{\partial X^2}+\frac{\partial^2 \theta}{\partial Y^2}+\frac{\partial^2 \theta}{\partial Z^2}\right) \tag{5}$$

Table 1
Basic geometrical parameters of heat sink.

Fin length L (mm)	51	Fin thickness t (mm)	1.5
Fin height H (mm)	10	Fin spacing δ (mm)	5
Fin number N	9	Pin height H_1 (mm)	10

Table 2
Four types of PPFHS.

Type	Diameter of pin fins (mm)		
	Pin-1	Pin-2	Pin-3
Type-1	1	1	1
Type-2	1	1	2
Type-3	1	2	2
Type-4	2	2	2

For the solid region of the plate pin fin heat sink, the steady state energy equation is

$$\frac{\partial^2 \theta}{\partial X^2}=0. \tag{6}$$

In this formulation the heat flux from the electronic chip is regarded as a boundary condition to the heat sink, and is different from Ref. [22], where it is treated as a heat generation in the solid heat sink. In the above equations, the dimensionless parameters are set as follows:

$$X=\frac{x}{Dh},\ Y=\frac{y}{Dh},\ Z=\frac{z}{Dh},\ U=\frac{u}{u_{\mathrm{in}}},\ V=\frac{v}{u_{\mathrm{in}}},$$
$$P=\frac{p}{\rho u_{in}},\ W=\frac{w}{u_{\mathrm{in}}},\ \theta=\frac{T_f-T_{\mathrm{in}}}{T_w-T_{\mathrm{in}}}$$

The pressure drop (Δp) from the inlet to the outlet of the flow passage, which reflects the hydraulic performance of the heat sink, is calculated by

$$\Delta p=p_{in}-p_{out} \tag{7}$$

The thermal resistance of the heat sink can be defined as [22]:

$$R_{th}=\Delta T/Q \tag{8}$$

where, ΔT stands for the difference between the highest temperature on the fin base and the ambient air temperature, and Q is the heating power that is employed upon the fin base of the heat sink. Thermal resistances of different heat sinks are analyzed to compare their thermal performances.

The pumping power which is required to support the heat sink can be calculated as by Sparrow and Ramsey [25]:

$$E=(\dot{m}/\rho)\Delta p=U_{\mathrm{in}}A_p\Delta p \tag{9}$$

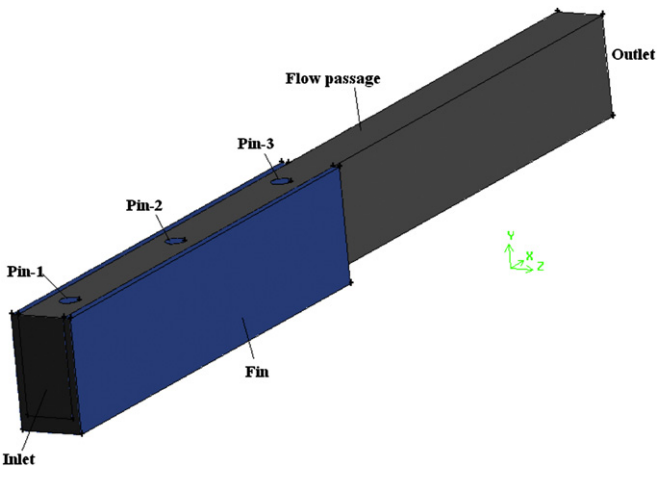

Fig. 2. Computation domain.

$$A_p = H\delta(N-1). \quad (10)$$

Here, H is the height of the fin, δ is the fin spacing, and N is the number of fins.

In order to optimize the configuration of the PPFHS, overall comparisons are necessary among different types of the PPFHS. In this part of the simulation, the temperature of the heat sink remains at 333 K and for comparison, the profit factor J, is defined as [24]

$$J = Q/E \quad (11)$$

2.4. Boundary conditions

In order to compare the simulation results to the existing simulation and experimental results shown in [24,26,27], the downstream boundary is located at a distance L from the fin edge in the x-direction in order to avoid backflow effects. The boundary conditions of velocity inlet and pressure outlet are assumed uniform in this simulation. The two side walls are set as symmetric taking advantage of the periodic structure assumption. All confined walls, except for the heating area, are assumed to be under no slip and adiabatic conditions. In addition, for conjugate simulation, the heat transfer between the surfaces of fin and base, and the fluid is specified as a coupled wall condition, through which the process occurs automatically without any outside intervention. Detailed description of boundary conditions in mathematical expressions is listed as follows:

At the inlet:

$$U = 1, \theta = 1 \quad (12)$$

At the outlet:

$$P = P_{out}, \frac{\partial\theta}{\partial n} = 0 \quad (13)$$

At the fluid–solid interface:

$$U = 0, \theta = \theta s, -k_s\frac{\partial\theta_s}{\partial n} = -k\frac{\partial\theta}{\partial n} \quad (14)$$

At the bottom plate (heating area):

$$q_w = -k_s\frac{\partial\theta_s}{\partial n} \quad (15)$$

At the top of the heat sink:

$$U = 0, \frac{\partial\theta}{\partial n} = 0 \quad (16)$$

2.5. Numerical method

A general purpose computational fluids dynamics (CFD) code, FLUENT 6.3.26, is chosen for the fluid dynamics and heat transfer simulation of the PPFHS. It is a state-of-the-art CFD software for complex geometries, and provides a wide range of turbulent models. The code uses the semi-implicit method for pressure linked equations (SIMPLE) algorithm [30] based on a control-volume application and using a pressure-based solver. The discrete schemes are QUICK with three order precision. Convergence is regarded to be achieved when the normalized residual errors of the continuity equation, energy equation, momentum equation and k–ε equations are less than 10^{-5}, 10^{-8}, 10^{-3} and 10^{-3}, respectively at the same time.

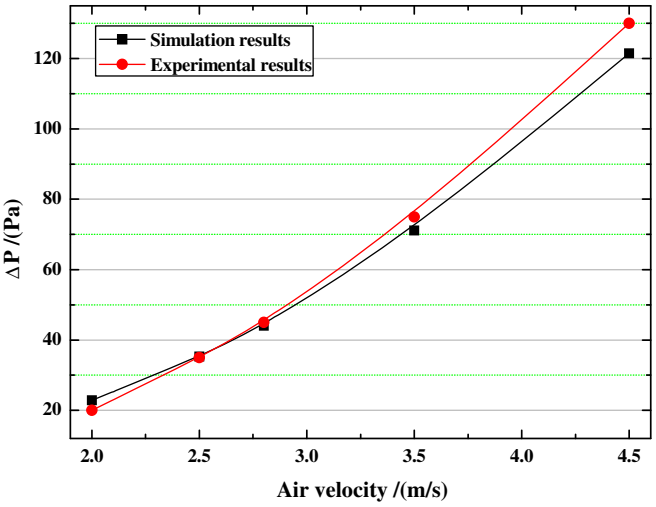

Fig. 3. Comparison of simulation and experimental pressure drop results.

3. Validation with experiment

In order to validate the numerical model, we use the experimental data from Yu et al. [27]. Adopting the geometrical structure

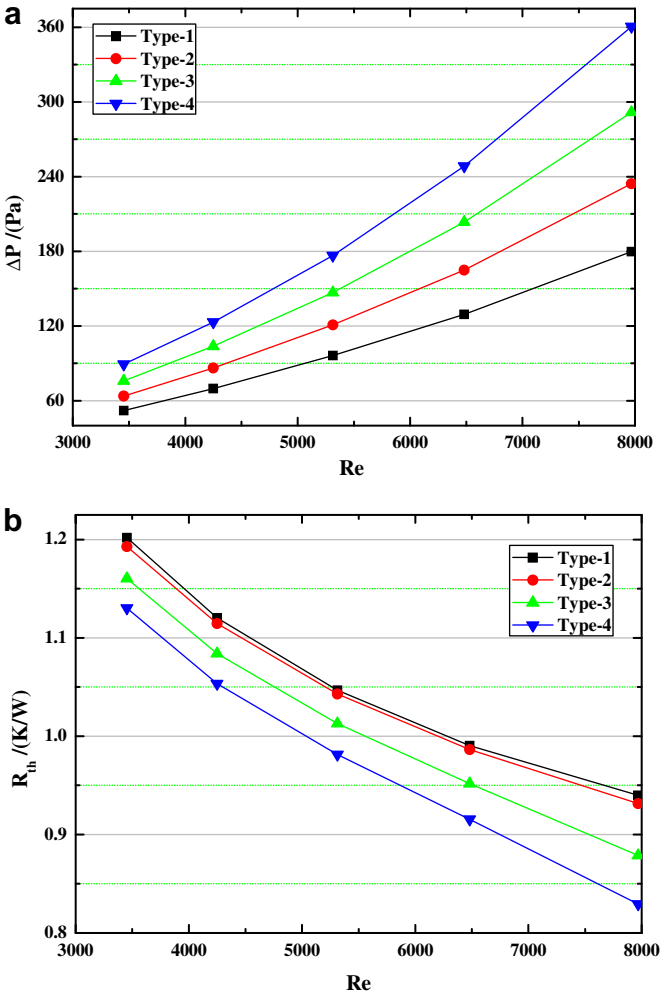

Fig. 4. Comparison of PPFHS with different pin–diameter combinations: in-line case. (a) The influence of air velocity on pressure drop (b) The influence of air velocity on thermal resistance.

of the experiment, simulation results are obtained for pressure drops at fluid velocities ranging from 2 m/s to 4.5 m/s. The results in Fig. 3 show less than 10% deviations between simulation and experimental results. Generally, the error is a little better than the validation results in Ref. [24], because we have considered the near-wall region influence and made finer meshes in these regions. The deviations between simulation and experimental results may be due to the neglect of the variation of fluid properties with temperature and the radiation heat transfer between the heat sink and the ambience. But the deviations are not so large, and thus the numerical results of PPFHS in the present work can be regarded as reasonable.

For testing grid independence, three mesh-models with different numbers for the staggered PPFHS with an NPFDCD of 24 mm are adopted to analyze the effect of mesh number on the numerical simulation results. The results indicate that the computed results based on 172,618 cells are insensitive to further grid refinement, and is thus employed for all models in the present study.

4. Results and discussions

Five inlet velocities (u_{in}) of 6.5, 8, 10, 12.2 and 15 m/s, corresponding to the *Re* number to be 3450, 4250, 5300, 6480, 7970, respectively are adopted to analyze the thermal and hydraulic performances of PPFHS shown in Figs. 4–8. Both staggered and in-line cases are investigated and the results are compared and analyzed.

4.1. Comparison of PPFHS with different pin–diameter combinations

In Figs. 4 and 5, comparisons amongst PPFHSs with different pin–diameter combinations are presented. It can be seen that when the *Re* number increases, larger pressure drops are acquired, while the thermal resistances of the heat sinks decrease dramatically. Furthermore, the PPFHSs listed in descending order of pressure drop are Type-4, Type-3, Type-2 and Type-1. On the other hand, the Type-1 PPFHS has the biggest thermal resistance, followed by Type-2, Type-3 and Type-4. The trends are identical in in-line and staggered cases shown in Fig. 5. This is because the airflow becomes more turbulent owning to the thicker pins, and the heat transfer is thus enhanced. At the same time, the pressure drop, i.e., the flow resistance, is raised, which means a larger pumping power is needed. It is also noticed that when the same *Re* number is employed, staggered cases have higher pressure drops and smaller thermal resistances than in-line cases.

Comparisons of the profit factors (J) with different heat sinks are depicted in Fig. 6. It is clear that the profit factor is higher under smaller *Re* number. The results also suggest that Type-1 PPFHS enjoys a higher profit factor, and therefore superior to the other

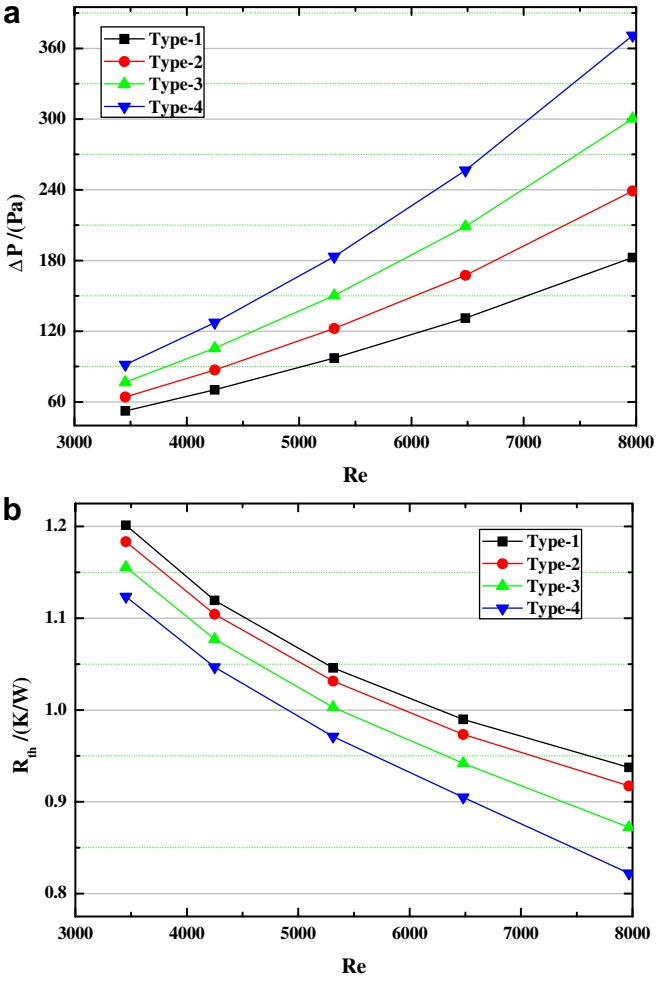

Fig. 5. Comparison of PPFHS with different pin–diameter combinations: staggered case. (a) The influence of air velocity on pressure drop (b) The influence of air velocity on thermal resistance.

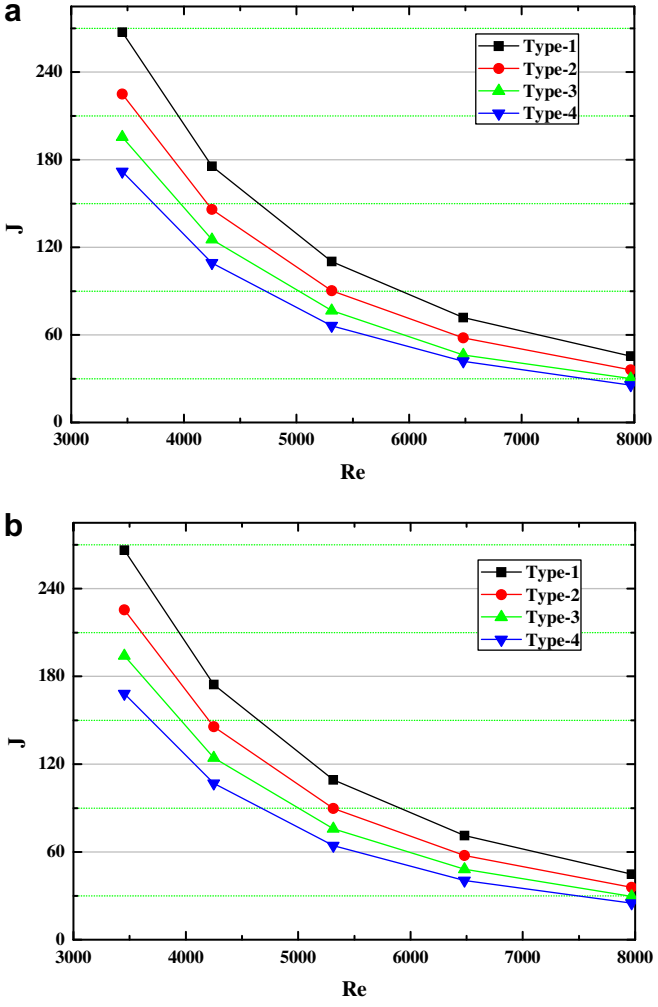

Fig. 6. Comparisons of the profit factors with different heat sinks. (a) In-line cases (b) Staggered cases.

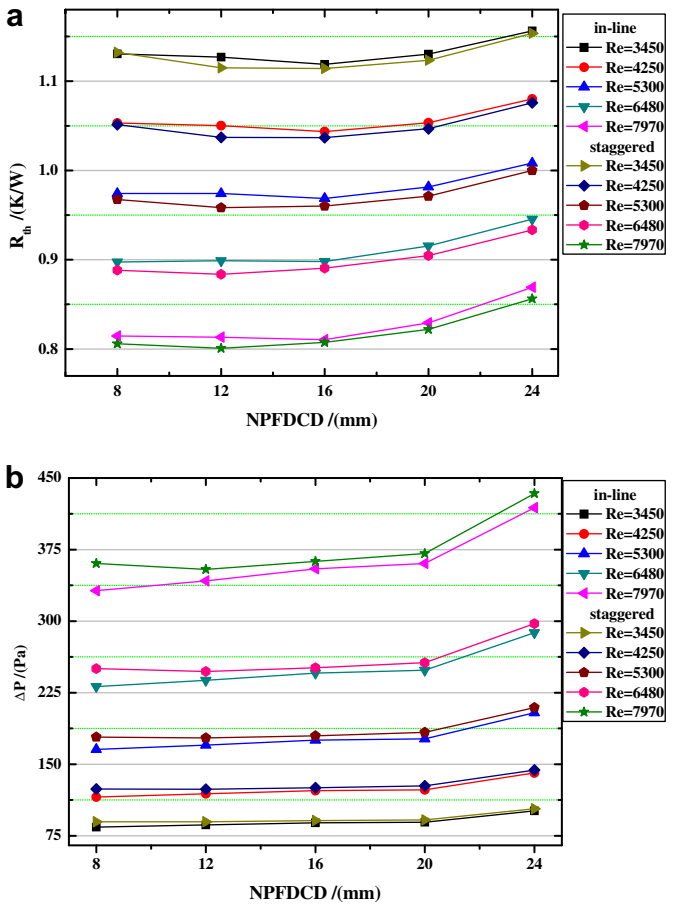

Fig. 7. Comparisons of PPFHS with different types and different air velocity (a) The influence of NPFDCD on thermal resistance (b) The influence of NPFDCD on pressure drop.

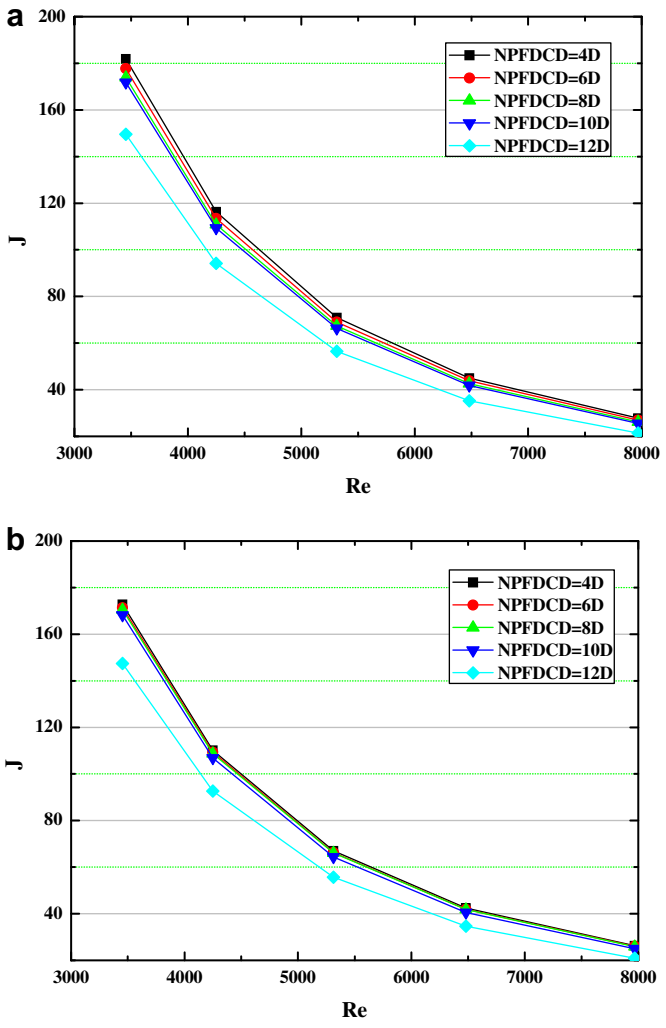

Fig. 8. Comparisons of the profit factors with different heat sinks (a) In-line cases (b) Staggered cases.

types. On the other hand, when in-line cases and staggered cases are compared, the former enjoys a higher profit factor than the latter. But from these results, the differences between in-line and staggered cases, with other parameters and working conditions remaining the same, are not so noticeable; less than 10%.

From the above results, we find that pin diameter and *Re* number have significant influences on the thermal and hydraulic performances of PPFHS. Larger pin diameter and higher air velocity can result in more drastic turbulent flow and larger pressure drop and lower thermal resistance, but lower profit factor. Whereas, the influence of in-line versus staggered arrays is not so notable.

4.2. Comparison of PPFHS with different NPFDCDs

In Fig. 7, PPFHS with different NPFDCDs (4D, 6D,8D, 10D and 12D) are compared under different *Re* numbers (3450, 4250, 5300, 6480, 7970, which means air velocities are 6.5, 8, 10, 12.2 and 15 m/s, respectively). It can be seen that when the NPFDCD increases, both in-line and staggered cases experience an increment in pressure drop. The thermal resistances first decrease, and then increase with increasing NPFDCD. It reaches its minimum value when NPFDCD is between 12 mm and 16 mm. One notable fact is that the thermal resistance represents dramatic increment when NPFDCD reaches 16 mm. According to the researches involving flow around cylinders [31], the vortexes caused by the cylinders are distributed in a ribbon-shaped downstream area, making the fluid in this certain area turbulent. A possible explanation of the phenomenon above is that when NPFDCD gets bigger, it exceeds the length of the ribbon-shaped area, leaving a less turbulent area between the ribbon-shaped area and the next cylinder, in which heat transfer is not effectively enhanced. Thus the thermal resistance becomes bigger. However, it should be noticed that the changes of both the thermal resistance and pressure drop are small. Furthermore, staggered cases have higher pressure drops and smaller thermal resistances than in-line cases under the same *Re* number.

Comparisons of the profit factors with different kinds of heat sinks are shown in Fig. 8. It is clear that with the increase of *Re* number, the profit factors of PPFHS with both in-line and staggered arrays decrease significantly, while increasing the NPFDCD reduces the profit factor (J) in both in-line and staggered cases. It can also be seen that with the NPFDCD changing from 4D to 10D, the variations of J at a given *Re* number are quite small, which leads to the conclusion that the influence of NPFDCD on the overall performance of PPFHS is limited. It should be noticed that when the NPFDCD is 12D, the profit factors for both in-line and staggered arrays decrease significantly. The reason for this can be found in Fig. 7, where both the thermal resistance and the pressure drop increase remarkably with the NPFDCD being 12D. Hence, increasing the NPFDCD does not have the significant benefit of improving the performance of the PPFHS. In addition, we can also see that the profit factors of in-line cases are a little higher than those of staggered cases, but the differences are neglected.

4.3. Applications of the PPFHS in desktop CPU

In this part of simulation, heating power of 10, 20, 40, 60 and 80 W, that is, heat fluxes at the fin base being 0.37, 0.73, 1.47, 2.20 and 2.93 W/cm^2, respectively, are employed on the Type-4 PPFHS mentioned above. The objectives are to analyze the possibility of application to the desktop PC CPU for waste heat dissipation, and secondly to estimate the tolerance of the heating power. It should be noted that, the heating powers of the simulation are selected according to the real working conditions of the PC CPU. As stated above, when the heating power is 10 W, the effect of the air temperature rise inside the flow passage on the air properties can be neglected. However, when the heating power is above 20 W, the effect of temperature on the air properties could no longer be neglected. A piecewise-linear method is thus adopted to depict the variations of air properties. The pressure drop and the highest temperature on the fin base are studied.

As shown in Fig. 9(a) and Fig. 10(a), when the heating power increases, the pressure drop of PPFHS changes very little, and it results mainly from the variations of the air properties. With increasing power, the air temperature will increase, which will result in an increase in air viscosity. Higher air viscosity will cause higher pressure drop under otherwise identical working conditions. On the other hand, from Fig. 9 (b) and Fig. 10 (b), the peak temperature on the fin base changes dramatically with the increasing heating power while decreases slightly with the increasing *Re* number. As we know, the MEMS can only work properly within a certain temperature range. Take the desktop PC CPU as example, the chip surface temperature has to be no more than 358 K (85 °C) [24], otherwise there is increased risk of instability or crash. In Fig. 9 (b) and Fig. 10 (b), a bold red line is used to indicate the temperature limit of desktop PC CPU. It can be seen that when the heating power to the fin base is 60 W (heat flux 2.20 W/cm^2) and air velocity is 6.5 m/s, the peak temperature on the fin base would still be under the required temperature limit. Thus PPFHS should be able to meet the cooling needs of a desktop PC CPU. However, it should be pointed that when the power is 80 W (2.93 W/cm^2), it requires an air velocity of 15 m/s to keep the peak temperature below the limit of 358 K. This means that when the power is too high, the working condition of PPFHS is tough: requiring higher air velocity, to be effected by higher pumping power.

In addition, the results of the numerical simulation for the cooling of desktop PC CPU by using other three types of PPFHSs shown in Table 2 indicates that each type of PPFHS can meet the cooling needs of a desktop PC CPU when the heating power is less than 60 W (heat flux less than 2.20 W/cm^2), with the air velocity larger than 6.5 m/s (*Re* = 3450).

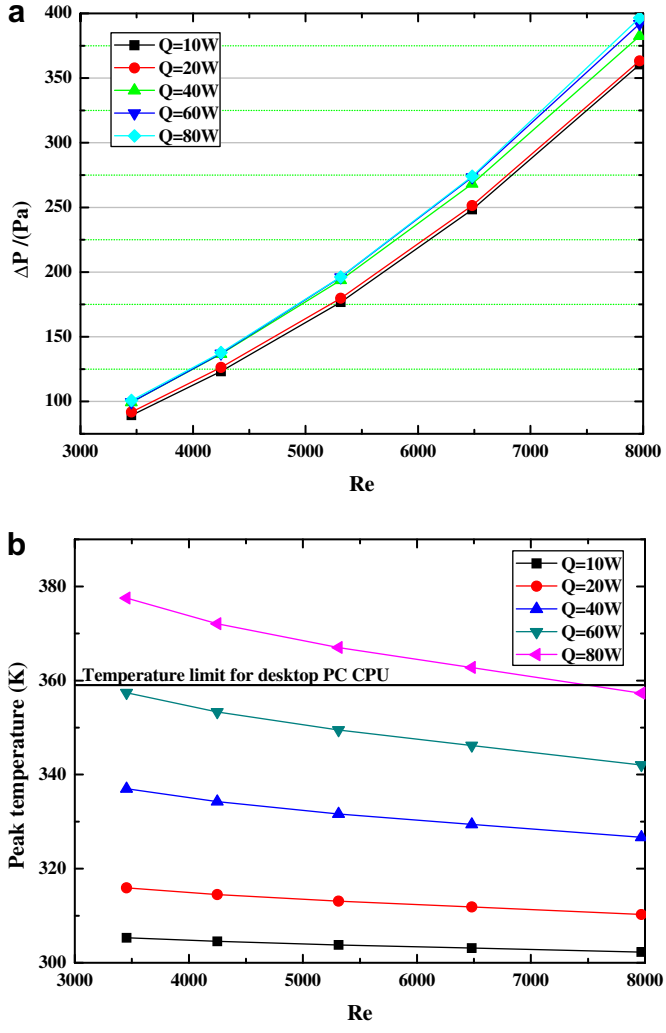

Fig. 9. Comparison of PPFHS under different heating power: in-line case. (a) The influence on pressure drop. (b) The influence on the fin-base peak temperature.

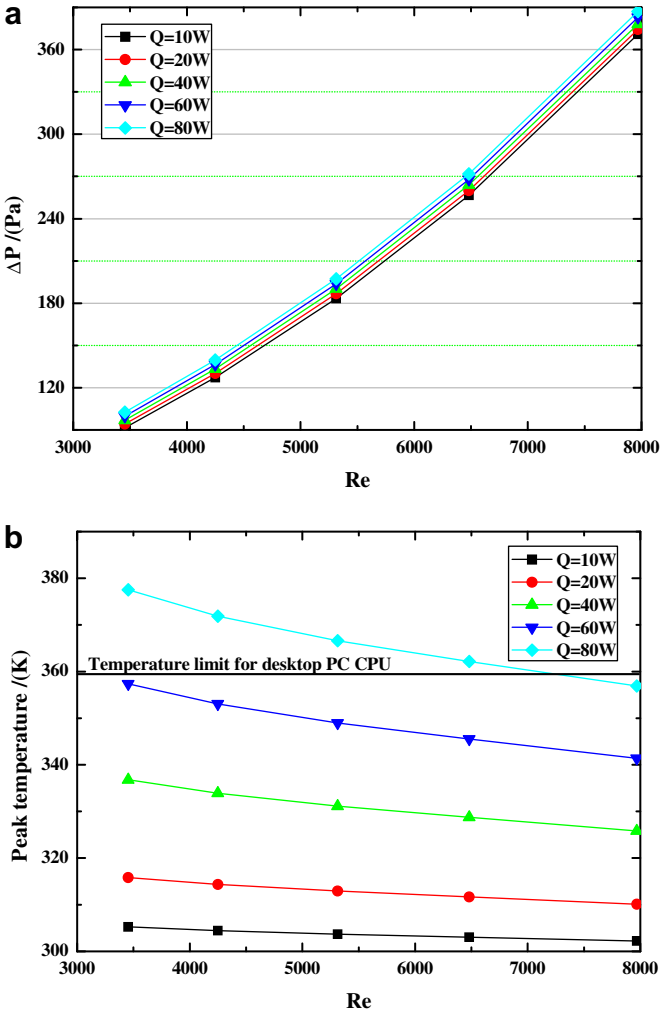

Fig. 10. Comparison of PPFHS under different heating power: staggered case. (a) The influence on pressure drop. (b) The influence on the fin-base peak temperature.

5. Conclusions

In this study, detailed analysis on the influences of air velocity, pin diameter, pin array, NPFDCD on the hydraulic and thermal performances of PPFHS has been conducted by conjugate numerical simulations using the commercial software Fluent 6.3.26. Furthermore, the potential industrial application of four types of PPFHS to the desktop PC CPU has also been explored. The four conclusions are:

(1) *Re* number (air velocity) is a key flow parameter in the performance of PPFHS. The flow resistance will increase significantly, and the thermal resistance and profit factor will decrease significantly, both with increasing *Re* number.
(2) Pin diameter is a key geometrical parameter in the performance of PPFHS. With increasing pin diameter, the flow resistance will notably increase, and the thermal resistance and profit factor will notably decrease.
(3) The influences of in-line versus staggered array and NPFDCD on the performance of PPFHS are not noticeable. The commercial design for the PPFHS need not emphasize on them.
(4) The proposed four types of PPFHS in this paper can all meet the cooling requirement of a desktop PC CPU with heating power less than 60 W and maximum temperature of 358 K.

Acknowledgements

This research was supported by the National Natural Science Foundation of China (51106060), the China Postdoctoral Science Foundation Fourth Special Funded Project (201104460) and the HUST Innovative Foundation (2011TS076).

References

[1] Z. Zhao, C.T. Avedisian, Enhancing forced air convection heat transfer from an array of parallel plate fins using a heat pipe, Int. J. Heat Mass Transf. 40 (13) (1997) 3135–3147.
[2] K.S. Kim, M.H. Won, J.W. Kim, B.J. Back, Heat pipe cooling technology for desktop PC CPU, Appl. Thermal Engng. 23 (9) (2003) 1137–1144.
[3] Y.M. Chung, K.H. Luo, Unsteady heat transfer analysis of an impinging jet, J. Heat Transf. 124 (6) (2002) 1039–1048.
[4] K. Nishino, M. Samada, K. Kasuya, K. Torii, Turbulence statistics in the stagnation region of an axisymmetric impinging jet flow, Int. J. Heat Fluid Flow 17 (3) (1996) 193–201.
[5] C.P. Tso, G.P. Xu, K.W. Tou, An experimental study of forced convection heat transfer from flush-mounted discrete heat sources, J. Heat Transf. 121 (2) (1999) 326–332.
[6] C.P. Tso, K.W. Tou, G.P. Xu, Flow boiling CHF of FC-72 from flush mounted and protruded simulated chips in a vertical channel, Int. J. Multiph. Flow 26 (3) (2000) 351–365.
[7] D.B. Tuckerman, R.F. Pease, High performance heat sinking for VLSI, IEEE Electr. Device Lett. 15 (5) (1981) 126–130.
[8] W. Qu, I. Mudawar, Experimental and numerical study of pressure drop and heat transfer in a single-phase micro-channel heat sink, Int. J. Heat Mass Transf. 45 (12) (2002) 2549–2565.
[9] K.T. Chiang, C.C. Chou, N.M. Liu, Application of response surface methodology in describing the thermal performances of a pin-fin heat sink, Int. J. Therm. Sci. 48 (2009) 1196–1205.
[10] H. Cao, G. Chen, Optimization design of microchannel heat sink geometry for high power laser mirror, Appl. Thermal Engng 30 (13) (2010) 1644–1651.
[11] Y.P. Chen, C.B. Zhang, M.H. Shi, J.F. Wu, Three-dimensional numerical simulation of heat and fluid flow in noncircular microchannel heat sinks, Int. Commun. Heat Mass Transf. 36 (9) (2009) 917–920.
[12] O. Leon, G.D. Mey, E. Dick, Study of the optimal layout of cooling fins in forced convection cooling, Microelectron. Reliab. 42 (7) (2002) 1101–1111.
[13] H.A. Mohammed, P. Gunnasegaran, N.H. Shuaib, Influence of channel shape on the thermal and hydraulic performance of microchannel heat sink, Int. Commun. Heat Mass Transf. 38 (4) (2011) 474–480.
[14] H.A. Mohammed, P. Gunnasegaran, N.H. Shuaib, Numerical simulation of heat transfer enhancement in wavy microchannel heat sink, Int. Commun. Heat Mass Transf. 38 (1) (2011) 63–68.
[15] C.C. Wang, K.S. Yang, Y.P. Liu, I.Y. Chen, Effect of cannelure fin configuration on compact air cooling heat sink, Appl. Thermal Engng. 31 (10) (2011) 1640–1647.
[16] M. Reyes, J.R. Arias, A. Velazquez, J.M. Vega, Experimental study of heat transfer and pressure drop in micro-channel based heat sinks with tip clearance, Appl. Thermal Engng. 31 (5) (2011) 887–893.
[17] Huibin Yin, Xuenong Gao, Jing Ding, Zhengguo Zhang, Experimental research on heat transfer mechanism of heat sink with composite phase change materials, Energy Conv. Manag. 49 (6) (2008) 1740–1746.
[18] R. Sabbah, M.M. Farid, S. Al-Hallaj, Micro-channel heat sink with slurry of water with micro-encapsulated phase change material: 3D-numerical study, Appl. Thermal Engng. 29 (2–3) (2009) 445–454.
[19] M.R. Shaeri, M. Yaghoubi, Thermal enhancement from heat sinks by using perforated fins, Energy Conv. Manag. 50 (5) (2009) 1264–1270.
[20] X.L. Xie, X.L. He, W.Q. Tao, H.W. Yang, An experimental investigation on a novel high-performance integrated heat pipe–heat sink for high-flux chip cooling, Appl. Thermal Engng. 28 (5–6) (2008) 433–439.
[21] T. Liang, Y. Hung, Experimental investigation oon the thermal performance and optimization of heat sink with U-shape heat pipes, Energy Conv. Manag. 51 (11) (2010) 2109–2116.
[22] H. Li, K. Chen, M. Chiang, Thermal-fluid characteristics of plate-fin heat sinks cooled by impingement jet, Energy Conv. Manag. 50 (11) (2009) 2738–2746.
[23] C.J. Ho, L.C. Wei, Z.W. Li, An experimental investigation of forced convective cooling performance of a microchannel heat sink with Al_2O_3/water nanofluid, Appl. Thermal Engng. 30 (2–3) (2010) 96–103.
[24] X.L. Yu, J.M. Feng, Q.K. Feng, Q.W. Wang, Development of a plate-pin fin heat sink and its performance comparisons with a plate fin heat sink, Appl. Thermal Engng. 25 (2–3) (2005) 173–182.
[25] E.M. Sparrow, J.W. Ramsey, C.A.C. Altemani, Experiments on in-line pin fin arrays and performance comparisons with staggered arrays, J. Heat Transf. 102 (1) (1980) 44–50.
[26] X.L. Yu, Q.K. Feng, Q.P. Liu, Research on the heat transfer and flow performance of a composite heat sink, J. Xi'an Jiaotong Univ. 37 (7) (2003) 670–673.
[27] X.L. Yu, Q.K. Feng, J.M. Feng, Research on thermal performance of plate-pin fin heat sink, J. Xi'an Jiaotong Univ. 38 (11) (2004) 1114–1118.
[28] Y.T. Yang, H.S. Peng, Investigation of planted pin fins for heat transfer enhancement in plate fin heat sink, Microelectron. Reliab. 49 (2) (2009) 163–169.
[29] M.A. Ismail, M.Z. Abdullah, M.A. Mujeebu, A CFD-based experimental analysis on the effect of free stream cooling on the performance of micro processor heat sinks, Int. Commun. Heat Mass Transf. 35 (2008) 771–778.
[30] S.V. Patankar, Numerical Heat Transfer and Fluid Flow, Hemisphere, Washington DC, 1980.
[31] Y.L. Wang, Y.Z. Liu, G.P. Miu, Three dimensional simulation of flow around cylinders, J. Shanghai Jiaotong Univ. 35 (10) (2001) 1465–1469.